Dynamical Aspects of Wintertime Cold-Air Pools in an Alpine Valley System

GÜNTHER ZÄNGL

Meteorologisches Institut der Universität München, Munich, Germany

(Manuscript received 30 November 2004, in final form 2 March 2005)

ABSTRACT

This study presents high-resolution numerical simulations in order to examine the dynamical mechanisms controlling the persistence of wintertime cold-air pools in an Alpine valley system. First, a case study of a cold-pool episode is conducted, the formation of which was related to the passage of a warm front north of the Alps. While the preexisting cold air was rapidly advected away in the Alpine foreland, a persistent cold pool was maintained in the inner-Alpine part of the valley system, associated with sustained horizontal temperature differences of up to 10 K over a distance of 30 km. The case study is complemented by a series of semi-idealized simulations, combining realistic topography with idealized large-scale flow conditions. These simulations consider a range of different ambient wind directions in order to investigate their impact on the cold-pool persistence.

The results indicate that the most important dynamical mechanism controlling the persistence of cold-air pools in deep Alpine valleys is cold-air drainage toward the Alpine foreland. The preferred direction for such a drainage flow is down the pressure gradient imposed by the (geostrophically balanced) ambient flow. Thus, for a given valley geometry and a given strength of the ambient flow, the probability for persistent cold-air pools mainly depends on the ambient wind direction. If the direction of the imposed pressure gradient matches a sufficiently wide connection to the foreland (a valley or a low pass), then a drainage flow will lead to a rapid removal of the cold air. However, the presence of pronounced lateral constrictions in the connecting valley may strongly reduce the drainage efficiency. Cold-pool erosion by turbulent vertical mixing seems to play a comparatively minor role in deep valley systems as considered in this study.

1. Introduction

Cold-air pools, most generally defined as a surface-based atmospheric layer with high static stability (not necessarily a temperature inversion), can form due to both radiative and dynamical processes. Among the radiative processes, one may distinguish between longwave radiative cooling under clear-sky conditions and reduced daytime heating due to a high surface albedo (snow cover) and/or a persistent low stratus deck. The basic dynamical formation process is advection of warmer air at higher levels, which may be related to subsidence and/or to quasi-horizontal advection of a warmer air mass (e.g., Zhong et al. 2001). The same basic distinction can be made for the processes capable of destroying a cold-air pool, where there is radiative heating and, among other dynamical mechanisms, turbulent vertical mixing. The most favorable locations for the formation of cold-air pools are basins and valleys, where the cold air produced over the surrounding slopes accumulates. Moreover, they tend to be sheltered from ambient winds, which reduces the effectiveness of the dynamical destruction mechanisms.

The majority of the existing literature on cold pools deals with radiative processes, for which only a brief overview is given here. Whiteman (1982) reported on detailed observations of the radiatively driven breakup of nocturnal temperature inversions, which were used by Whiteman and McKee (1982) to develop and validate a simple thermodynamical model. This model basically conducts an energy budget calculation for a given valley geometry and turned out to provide fairly accurate results under synoptically undisturbed weather conditions. The next step of refinement already required using a full numerical model, which allowed Bader and McKee (1985) to investigate the effects of ambient shear and stability. The first simulations dedicated to study the formation of a cold pool in a basin were conducted by Vrhovec (1991), showing the

Corresponding author address: Günther Zängl, Meteorologisches Institut der Universität München, Theresienstraße 37, D-80333 München, Germany.
E-mail: guenther@meteo.physik.uni-muenchen.de

interplay between the slope winds and the growth of the surface inversion. More recently, Anquetin et al. (1998) conducted large-eddy simulations of the radiative formation and breakup of cold pools in a deep valley, and Colette et al. (2003) studied the effect of topographic shading in deep valleys. Moreover, a number of recent papers deal with the formation and breakup of extreme cold-air pools in closed mountain sinkholes (e.g., Clements et al. 2003; Whiteman et al. 2004).

The investigation of dynamical aspects related to cold pools started with Lee et al. (1989). They studied the interactions between gravity-wave-driven downslope winds and a leeside cold pool and found that the persistence of the cold pool depends quite sensitively on the leeside pressure field. If the leeside pressure gradient tends to push the cold air toward the mountain, no significant gravity waves can form because the ambient flow is prevented from penetrating down the lee slope. However, a downslope windstorm gradually develops if the leeside pressure field tends to advect the cold pool away from the mountain. The turbulent mixing on top of the cold pool, which could erode the cold pool in the absence of a favorable pressure gradient, was found to be quite ineffective. The fact that ambient winds have to be fairly strong to erode even a shallow cold pool was further established by Petkovšek (1992), Rakovec et al. (2002), and Zhong et al. (2003). For large basins, for example, the redistribution of the cold air mass due to a horizontal pressure gradient imposed on top of the cold pool (e.g., related to a geostrophically balanced ambient flow) might be more important than turbulent mixing for light to moderate wind speeds (Petkovšek and Vrhovec 1994; Zängl 2003a). Since the cold air tends to accumulate on that side of a basin where the ambient pressure is low, part of a basin might get out of the cold pool without the need of any turbulent mixing or radiative heating. Likewise, the persistence of a cold pool in a valley depends on whether the mesoscale pressure field favors a downvalley drainage of the cold air or not (Zängl 2003a). If, on the other hand, turbulent mixing plays a role, upstream blocking can be an important factor in determining if a cold pool gets eroded or not (Zängl 2003a). Finally, cold-air advection aloft can terminate the existence of a cold pool (Zhong et al. 2001).

The primary limitation of most existing studies (except for Zhong et al. 2001) on dynamical aspects of cold pools is their restriction to idealized simulations or even analytical models. Though theoretical studies are undoubtedly important to obtain insight into the dynamical processes affecting the evolution of cold pools, they need to be complemented by realistic ones in order to assess what importance these processes have in reality. Since Zhong et al. (2001) focused on the evolution of a cold pool in a large basin (the Columbia basin), there presently exists no realistic study on the dynamics of cold pools in a complex system of Alpine valleys. It has not even been established to what extent current mesoscale models are able to simulate the strength and spatial extent of cold pools on a kilometer scale.

Making a first step toward closing these gaps will be the primary goal of the present paper. Specifically, we will investigate the evolution of a cold pool in a valley system called Salzkammergut, which is located in Austria close to the northern edge of the eastern Alps (see Fig. 1). The cold pool under consideration was generated by a warm-front passage from the west and was restricted to the inner-Alpine part of the valley system as the preexisting cold air was rapidly advected away in the Alpine foreland. The primary motivation for choosing the Salzkammergut region is its comparatively high density of hourly reporting operational surface stations, which is crucial for verifying the simulations given the high spatial variability of this type of event. The case study will be complemented by semi-idealized simulations combining the realistic topography with different large-scale flow conditions. The outline of the paper is as follows: After describing the setup of the experiments in section 2, the results of the case study will be presented in section 3. Section 4 focuses on a dynamical analysis of the event, including the above-mentioned semi-idealized simulations. The main results of this work will be summarized in section 5.

2. Model and setup

The numerical simulations presented in this study have been conducted with the fifth-generation Pennsylvania State University–National Center for Atmospheric Research Mesoscale Model (MM5, version 3.3) (Grell et al. 1995). The model solves the nonhydrostatic equations of motion in a terrain-following sigma coordinate system. Four interactively nested model domains are used, having a horizontal mesh size of 16.2 km, 5.4 km, 1.8 km, and 600 m, respectively. The corresponding numbers of grid points are 148×142, 166×127, 118×118, and 118×112, respectively. The area covered by the first domain is displayed in Fig. 1a together with the location of the nested domains, and a close-up view of the innermost domain is provided in Fig. 1b. The model topography was created from U.S. Geological Survey (USGS) digital elevation data with a resolution of 5′ (domain 1) and 30″ (domains 2–4). Information on land-use categories was also obtained from USGS data with the same resolution as the terrain data. In the

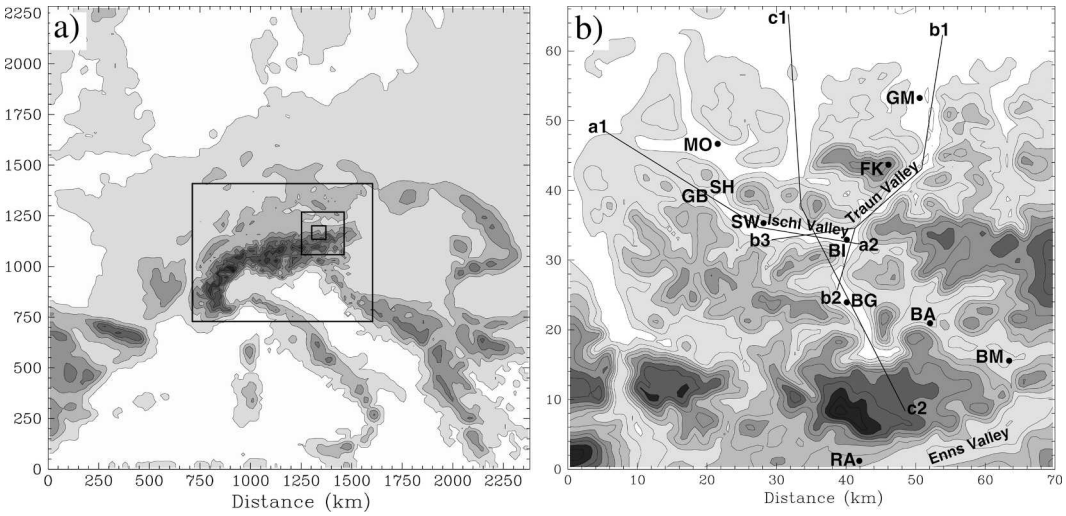

FIG. 1. (a) Topography of the coarse model domain and position of the nested domains (boxes). The contour and shading increment is 400 m, starting at sea level. (b) Topography of the fourth model domain. Shading starts at a height of 600 m with an increment of 400 m, and additional height contours are given every 200 m. Bold lines indicate the locations of vertical cross sections shown later in this paper (a1–a2, b1–b2, b1–b3, and c1–c2). Note that these cross sections have kinks in order to follow the valleys. Surface stations are located at Mondsee (MO), Gmunden (GM), Feuerkogel (FK), Sankt Wolfgang (SW), Bad Ischl (BI), Bad Goisern (BG), Bad Aussee (BA), Bad Mitterndorf (BM), and Ramsau (RA). In addition, SH and GB mark the location of small passes named Scharflingerhöhe and Gilgner Berg, respectively.

vertical, 41 full-sigma levels are used, corresponding to 40 half-sigma levels where all variables but the vertical wind are computed. The lowermost half-sigma level, which will be referred to as surface level in the remainder of this paper, is located about 10 m above ground. The vertical spacing between the model layers ranges between 30 m near the surface and 750 m near the upper model boundary, which is located at 100 hPa. At the upper boundary, a radiation condition is used to prevent spurious reflections of vertically propagating orographic gravity waves. The radiation condition is based on the work of Klemp and Durran (1983) and has been modified in order to enhance the range of horizontal wavelengths captured by it. In the standard MM5 implementation, this wavelength range is limited to 12 times the grid distance, which is clearly insufficient for the two inner model domains and might have spurious side effects on the interaction between orographic gravity waves and the cold pool under investigation. In the modified version, the longer wave components are interpolated from the coarser model domain(s), ensuring that the whole spectrum of gravity waves is able to radiate upward. A description of this procedure is given in the appendix of Zängl (2002a). It is mentioned that the local computation of the radiation condition is switched off in the innermost model domain since the wavelength range that would be radiated upward in this case (up to 7.2 km) is not able to propagate vertically under the atmospheric conditions considered in this study (see below). In the innermost model domain, only the interpolation of the radiation condition from the coarser domains is retained. This way, it is achieved that the vertically propagating part of the wave spectrum is radiated upward without applying the radiation condition to vertically decaying wave components.

The case-study simulation conducted in this study starts on 27 December 2001 at 1200 UTC and is integrated over 30 h. The initial and boundary data needed for this simulation are taken from the European Centre for Medium-Range Weather Forecasts (ECMWF) operational analyses. The data are used at an interval of 6 h on standard pressure levels and a $0.5° \times 0.5°$ latitude–longitude grid. It is mentioned that the available snow-cover data did not prove to be useful for this simulation although snow-cover effects probably had some impact on the local temperature field in the Alpine valleys. The problem lies in the fact that the spatial gradients of the snow coverage were too large in the present case to be properly represented by coarse-resolution analyses. While there was only a thin snow cover in the foreland, which rapidly melted during the event considered here, there were 30–60 cm of snow in the Alpine valleys and 100–200 cm on the mountains. This gradient being heavily smoothed in the available data, the initial simulation using the standard snow-cover module of MM5

exhibited a significant cold bias in the Alpine foreland because the excessive snow cover prevented the ground temperature from rising above the freezing point. Since the subsequent experiment without the snow-cover module showed a satisfactory agreement with the observed evolution, it has been decided to use this experiment for further discussion. In addition, a sensitivity test has been conducted in which the soil heat capacity was artificially halved in the Alpine valleys in order to mimic the effect of a fresh snow cover. This test showed only a minor, temporarily limited effect, and was stopped after 18 h of simulation.

To allow for a proper representation of the relevant physical processes, a full suite of physics parameterizations is used. Cloud microphysics are treated with the so-called Reisner2 scheme that has prognostic equations for cloud water, cloud ice, cloud ice particle number concentration, rain, snow, and graupel (Reisner et al. 1998). In the two outer model domains, a simple cumulus parameterization (Grell 1993) is used since convective instability may occur over the comparatively warm ocean areas. The planetary boundary layer is parameterized using the Gayno–Seaman scheme (Shafran et al. 2000), which integrates a prognostic equation for turbulent kinetic energy (TKE) and parameterizes vertical mixing as a function of the local TKE value. Moreover, a radiation scheme accounting for interactions with moisture and clouds (Grell et al. 1995; Mlawer et al. 1997) is used. Following the formulas given by Garnier and Ohmura (1968), it was modified by the author so as to include the effects of sloping topography and topographic shading on the flux of direct solar radiation. However, three-dimensional effects on longwave radiative transfer are not accounted for. Another important modification affects the implementation of the horizontal numerical diffusion, which is computed along the terrain-following sigma surfaces in the original MM5. Since this induces large systematic errors for variables having a strong vertical stratification, the diffusion is computed truly horizontally for the temperature and the mixing ratios of water vapor and cloud water in the modified version (Zängl 2002b). As demonstrated by Zängl (2003a), using this modified diffusion scheme is of crucial importance for a meaningful simulation of the evolution of cold-air pools. Finally, the generalized vertical coordinate described by Zängl (2003b) is used. It allows for a rapid decay with height of the topographic structures in the coordinate surfaces. The main advantage of this type of generalized coordinate is that horizontal advection over mountainous terrain becomes more accurate (see also Schär et al. 2002).

The semi-idealized simulations are conducted in dry mode without consideration of radiation effects. In these experiments, only the boundary layer parameterization is retained to account for the effects of surface friction. This configuration has been chosen to focus on dynamical processes, motivated by the fact that the relevant time period of the observed case was characterized by a closed cloud cover. The basic temperature profile used for the idealized runs starts with a sea level temperature of 9°C (282.15 K), followed by a tropospheric vertical gradient of -6.5 K km^{-1} up to a pressure of 250 hPa. Above this level, an isothermal stratosphere is assumed. At initial time, this basic profile is modified in the domain of interest in order to obtain a cold-air pool. Specifically, an isothermal gradient is prescribed below 850 hPa in the region 47–48°N, 12°–15°E, corresponding to a temperature deficit of about 6.5 K at valley level (500 m). The cold pool is surrounded by a 150-km-wide transition zone to avoid a shock-like spreading out of the cold air. The large-scale wind field is horizontally homogeneous throughout the model domain and involves positive shear. Except for the frictional boundary layer, it is in geostrophic balance with the pressure field, assuming a constant Coriolis parameter of 10^{-4} s^{-1} throughout the model domain. Through the thermal wind relation, the forward shear implies the presence of horizontal temperature gradients, so that the temperature values given above are strictly valid in the center of the model domain only. At initial time, the wind speed is set to 2.5 m s^{-1} at sea level and 17.5 m s^{-1} at tropopause level with linear shear in between and constant speed above the tropopause. In the core region of the cold pool, the initial wind speed is set to zero. During the first 6 h of the simulation, the wind speed is increased by 7.5 m s^{-1} through changing the conditions at the lateral model boundaries, yielding 10 and 25 m s^{-1} at sea level and tropopause level, respectively. Afterward, the large-scale wind field remains constant until the end of the simulations at $t = 24$ h. This acceleration procedure is similar to that used in Zängl (2003a) and is needed for a proper dynamical adjustment of the cold pool. The large-scale wind direction is constant throughout the model domain (apart from boundary layer effects) and is varied from 210° through 310° at an increment of 20°, yielding a total of six idealized simulations.

3. Case study of the 28 December 2001 event

a. Synoptic environment

The synoptic situation on the days under consideration was characterized by a deep anticyclone over the eastern Atlantic, leading to a mainly northwesterly midtropospheric flow over large parts of Europe. Following this midtropospheric steering flow, surface cy-

clones were moving from Iceland via Scotland toward the southern Baltic Sea. For the time period between 1800 UTC 27 December and 1800 UTC 28 December, Fig. 2 shows the sea level pressure, the geopotential at 500 hPa, and the wind and potential temperature fields at 925 hPa.

The event considered here was preceded by an intrusion of polar air toward the Alps that led to lee cyclogenesis in the Mediterranean Sea and to a strong bora windstorm along the Croatian Adriatic coast. At 1800 UTC on 27 December, the warm front related to another cyclone approaching from the North Sea is about to reach the Alps (Figs. 2a,b). The temperature increase associated with this warm front at 925 hPa is about 7 K. Ahead of the warm front, the low-level flow is southwesterly and has a strength of 15 to 20 m s^{-1} in the northern Alpine foreland (Fig. 2b). At higher levels, the flow turns to northwest or even north, consistent with the presence of warm-air advection (Fig. 2a). During the subsequent 12 h, the latter cyclone moves from Denmark to the Baltic Sea and weakens somewhat (Fig. 2c). At the same time, the next Atlantic cyclone enters the model domain from the northwest. At 0600 UTC on 28 December, its center is located east of Scotland (Fig. 2c). The Alpine region is now located in the warm sector, and the airflow is mainly west-northwesterly with only weak directional shear. At low levels, the airflow still has a southerly component in the northern Alpine foreland due to deflection effects (Fig. 2d).

By 1800 UTC on 28 December, the second cyclone has reached Denmark (Fig. 2e). Its cold front is located about 200 km north of the Alps, and one may notice that the winds behind the front are almost parallel to the orientation of the front (Fig. 2f). This implies that the front will not make much further progress toward the south. Moreover, it is interesting to note that a secondary cyclone is developing on the cold front, just entering the model domain from the west near $y = 1500$ km. It led to the formation of a pronounced, quasi-stationary airmass boundary on the following day, lingering approximately 150 km north of the Alps.

b. Evolution of the local temperature field

The observed evolution of the temperature field is presented in Fig. 3 for eight surface stations and the time period between 1600 UTC 27 December and 1800 UTC 28 December. The location of the stations is indicated in Fig. 1b except for Wolfsegg, which is located about 8 km north of the fourth model domain. Two of the stations marked in Fig. 1b (Mondsee and Bad Ischl) are not included here because they report only 3 and 4 times per day, respectively. For comparison, Fig. 3 also shows the simulated temperature time series for the respective stations. Note that this comparison starts only 4 h after the initialization of the model, which was found to be sufficient for a proper model spinup in the present case.

The station at the Feuerkogel mountain (Fig. 3a) approximately represents the temperature at the 850-hPa level (see Fig. 3 for station heights). At that level, a temperature jump by about 5 K occurred between 1600 and 2000 UTC on 27 December, followed by a gradual but almost continuous warming by another 6 K during the remaining 22 h of the time period considered here. For completeness, it is mentioned that the minimum temperature of 27 December, −12.8°C, was measured at 1300 UTC. As can be inferred from the observed dewpoint data (not shown), the initial rapid warming phase was related to subsidence, which is consistent with the southwesterly low-level flow present at that time (Fig. 2b). After 2100 UTC, the air humidity increased rapidly and reached almost saturation after midnight.

Wolfsegg, representing the conditions in the Alpine foreland, exhibits a slight cooling until 2000 UTC on 27 December, followed by an almost steady temperature increase from −7°C to +5°C during the rest of the time (Fig. 3a). The initial temperature decrease is due to radiative cooling; the clouds related to the frontal system reached the area under consideration between 2100 and 2200 UTC. Gmunden, located at the northern edge of the Alps, exhibits a similar temperature evolution as Wolfsegg, but the warming commences 2 h earlier, and the temperature level is generally higher (Fig. 3b). Note that only part of this temperature difference can be traced back to the lower altitude of Gmunden. Particularly in the late evening of 27 December, Gmunden even had a higher potential temperature than Wolfsegg. The vertical temperature gradient between the Feuerkogel and Gmunden is between dry adiabatic and moist adiabatic during most of the time, implying that no notable cold-air pool was present along the northern edge of the Alps. Farther north (e.g., at Wolfsegg), an appreciable cold pool formed in the evening of 27 December, but it was only of temporary nature as the approaching warmer air reached the surface in the morning of 28 December.

On the other hand, a pronounced and persistent cold-air pool was present in the Alpine valleys. The lowest temperatures are found at Bad Aussee and Bad Mitterndorf (Figs. 3e,f), followed by Bad Goisern (Fig. 3c). At these stations, pronounced radiative cooling took place until the arrival of the frontal clouds around 2200 UTC. Afterward, the temperatures increased

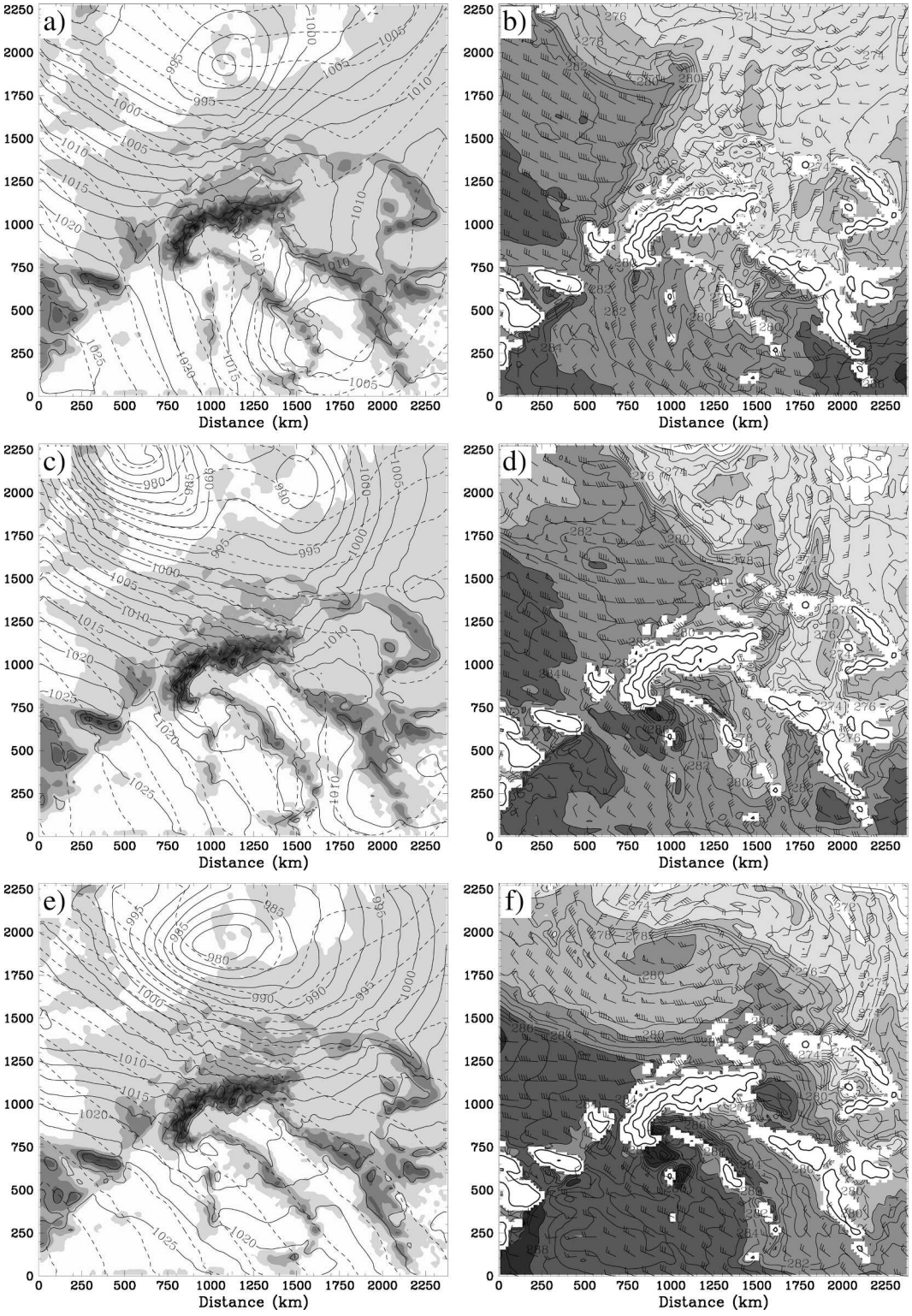

FIG. 2. Synoptic-scale fields at (a), (b) 1800 UTC 27 Dec; (c), (d) 0600 UTC 28 Dec; (e), (f) 1800 UTC 28 Dec. (left) Sea level pressure (solid lines; contour interval 2.5 hPa) and geopotential height at 500 hPa (dashed lines; contour interval 40 gpm). Topography is shaded as in Fig. 1a. (right) Horizontal wind (full barb = 5 m s^{-1}) and potential temperature (contours every 1 K; shading starts at 272 K with an increment of 4 K) at 925 hPa. Regions having a surface pressure below 925 hPa are hidden (appearing white), and smoothed topography contours are drawn for 1000 and 2000 m.

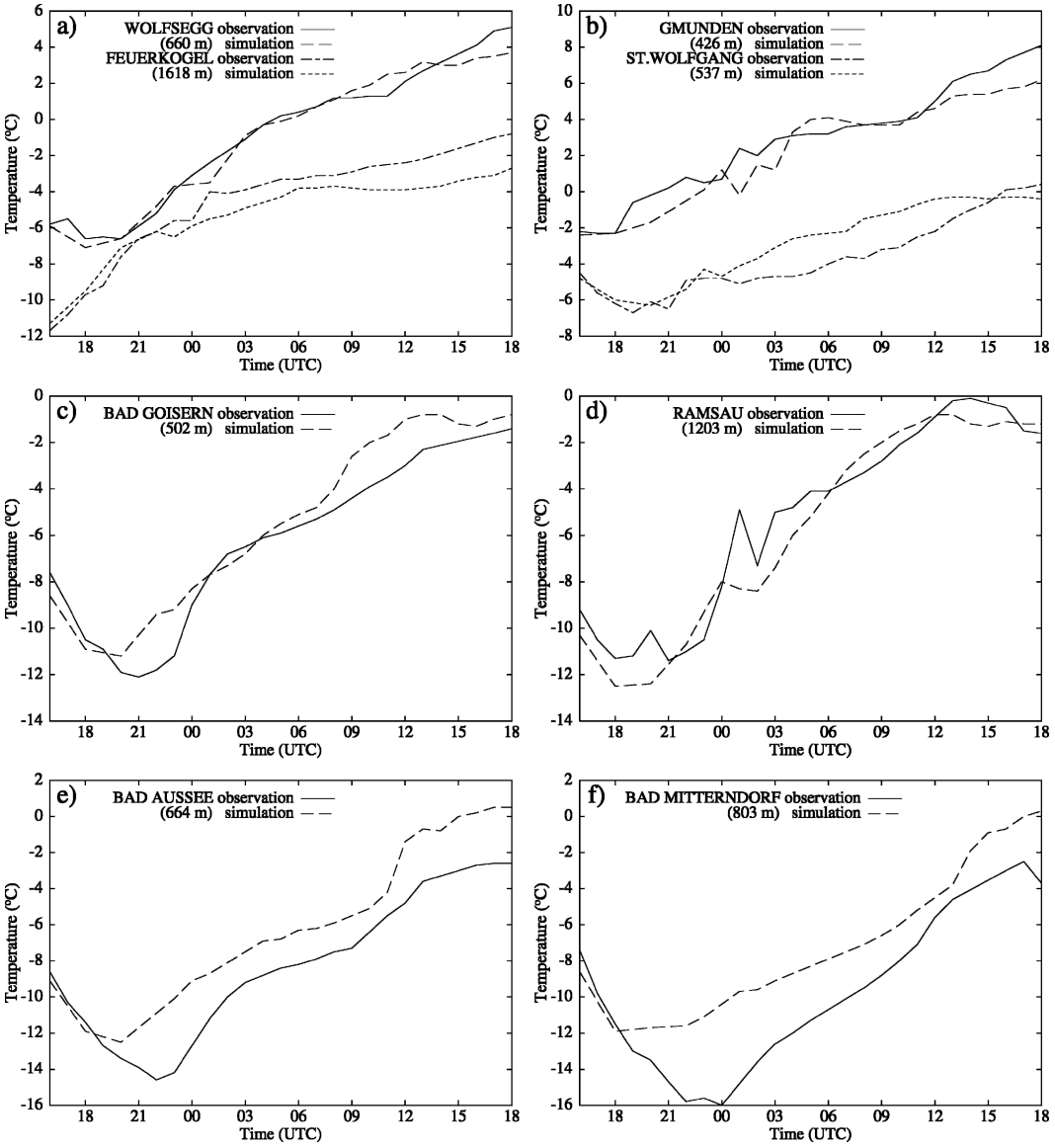

FIG. 3. Observed temperature evolution at eight surface stations between 1600 UTC 27 Dec and 1800 UTC 28 Dec, and comparison with the corresponding model results. The location of the stations is indicated in Fig. 1b except for (a) Wolfsegg, which lies 8 km north of the northern domain boundary at $x \approx 43$ km. Station heights are indicated in the figure panels.

more or less steadily but remained roughly 10 K lower than at Gmunden. This difference is particularly impressive for Bad Goisern, which is located only 75 m higher than Gmunden. A sustained cold pool is also found at St. Wolfgang (Fig. 3b), although this village is separated from the Alpine foreland by only one major mountain range. The initial radiative cooling is quite weak there due to the proximity of a fairly big lake, but nevertheless, the temperature difference between St. Wolfgang and Gmunden remains almost constant at 8 K throughout 28 December. Finally, the temperature readings at Ramsau (Fig. 3d) provide some information on the inner-Alpine temperature evolution at intermediate levels. Ramsau is located on a small plateau, about 450 m above the bottom of the Enns Valley, and is therefore not affected by local cold-air pools. A comparison with the Feuerkogel observations reveals a significant delay in the onset of the warming, which is related both to the lower height and to the distance from the northern Alpine edge. In contrast to the other stations, the major warming step shortly after midnight was discontinuous at Ramsau, indicating the temporary

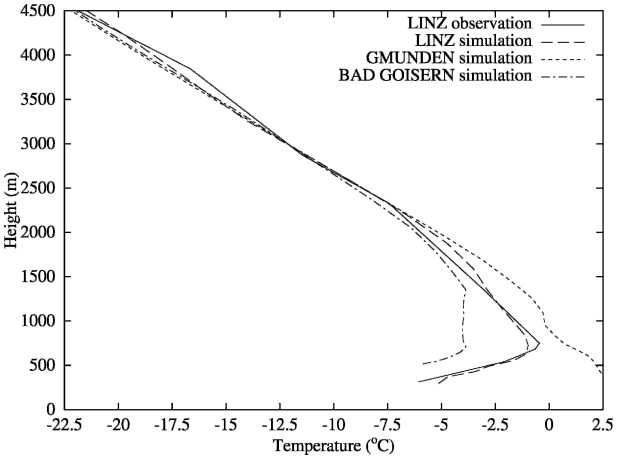

FIG. 4. Simulated and observed vertical temperature profiles at 0400 UTC 28 Dec.

presence of a sharp inversion oscillating around a height of 1200 m.

To illustrate the vertical structure of the temperature field, model-derived temperature profiles are displayed in Fig. 4 for Bad Goisern, Gmunden, and Linz, the latter being located 50 km northeast of Gmunden in the Danube Valley. Results are taken at 0400 UTC on 28 December because a radiosonde ascent is available for Linz at that time. The temperature profile for Bad Goisern shows a shallow surface inversion topped by a 700-m-deep isothermal layer. The upper boundary of the isothermal layer (1400 m) is slightly below the average crest level of the mountain ranges north of Bad Goisern. At higher levels, the temperature progressively decreases with height, reaching a vertical gradient of about -6.5 K km^{-1} above 2000 m. The temperature profile for Gmunden is consistently warmer than that for Bad Goisern below about 2500 m, the difference exceeding 1 K at heights below 2000 m. Except for a thin isothermal layer near the freezing level, which might be affected by melting precipitation, the low-level vertical temperature gradient above Gmunden ranges between moist and dry adiabatic. Farther out in the Alpine foreland, the temperature is colder again, and there is still a pronounced surface inversion in the Danube Valley. The surface inversion at Linz became dissolved in the late morning of 28 December (not shown).

A comparison of the observed temperature data with the corresponding model results demonstrates that the model performs sufficiently well to be useful for a closer investigation of this event. The best agreement is obtained in the Alpine foreland, where the difference between simulated and observed temperatures mostly ranges between -1 K and $+1$ K. This holds for the surface stations as well as for the radiosounding of Linz. At the Feuerkogel mountain, the model error is also below 1 K during most of the time, but a systematic cold bias up to 2 K emerges in the last 6 h of the simulation. This bias might be related to the developing airmass boundary (see Fig. 2f and related discussion), which is probably too smooth in the simulation because it is already smoothed in the ECMWF analysis data providing the lateral boundary conditions.[1] A very good agreement is also found for Ramsau except for a few hours after midnight where the discontinuous temperature evolution appears heavily smoothed in the model. At the inner-Alpine valley stations, the model tends to have some warm bias, but nevertheless, it reproduces 70%–90% of the observed temperature differences between the northern edge of the Alps (Gmunden) and the valley stations. Given the enormous spatial variability of the temperature field, this can still be regarded as a very satisfying performance. The most notable discrepancy between model results and observations occurs at Bad Goisern, Bad Aussee and Bad Mitterndorf, where the initial radiative cooling evidently stops too early in the simulation. A plausible explanation for this would be that the frontal clouds reach the Alps 2 or 3 h too early in the model, but a definitive verification of this hypothesis is difficult because only data from automatic weather stations are available at nighttime. Another factor that could contribute to the overestimation of the nocturnal temperature minima is the neglect of snow-cover effects in the simulation presented here. However, a sensitivity test in which the soil heat capacity was artificially halved in the Alpine valleys (but not over the forested mountain slopes) showed only a minor improvement ($\lesssim$1 K) until 2100 UTC.[2] Afterward, the surface temperatures rapidly approached those of the reference simulation, supporting the hypothesis of a timing error in the cloud cover.

Before turning to the analysis of the model results, we briefly mention that the simulated precipitation has also been verified against observations. At the inner-Alpine valley stations, the observed accumulated precipitation (1800 UTC 27 December–1800 UTC 28 December) ranges between 10 mm at Bad Mitterndorf and 16 mm at St. Wolfgang. Ramsau, being shaded by the Dachstein massif, registered only 5 mm. The simulated values tend to be somewhat larger than the observed ones but do not exceed 130% of the observed values

[1] The peak intensity this airmass boundary reached on the following day was a temperature jump of 7 K within less than 50 km. This is clearly beyond the capability of a global analysis scheme.

[2] The albedo effect is unimportant in this context because most valley segments are shadowed by 1330 UTC.

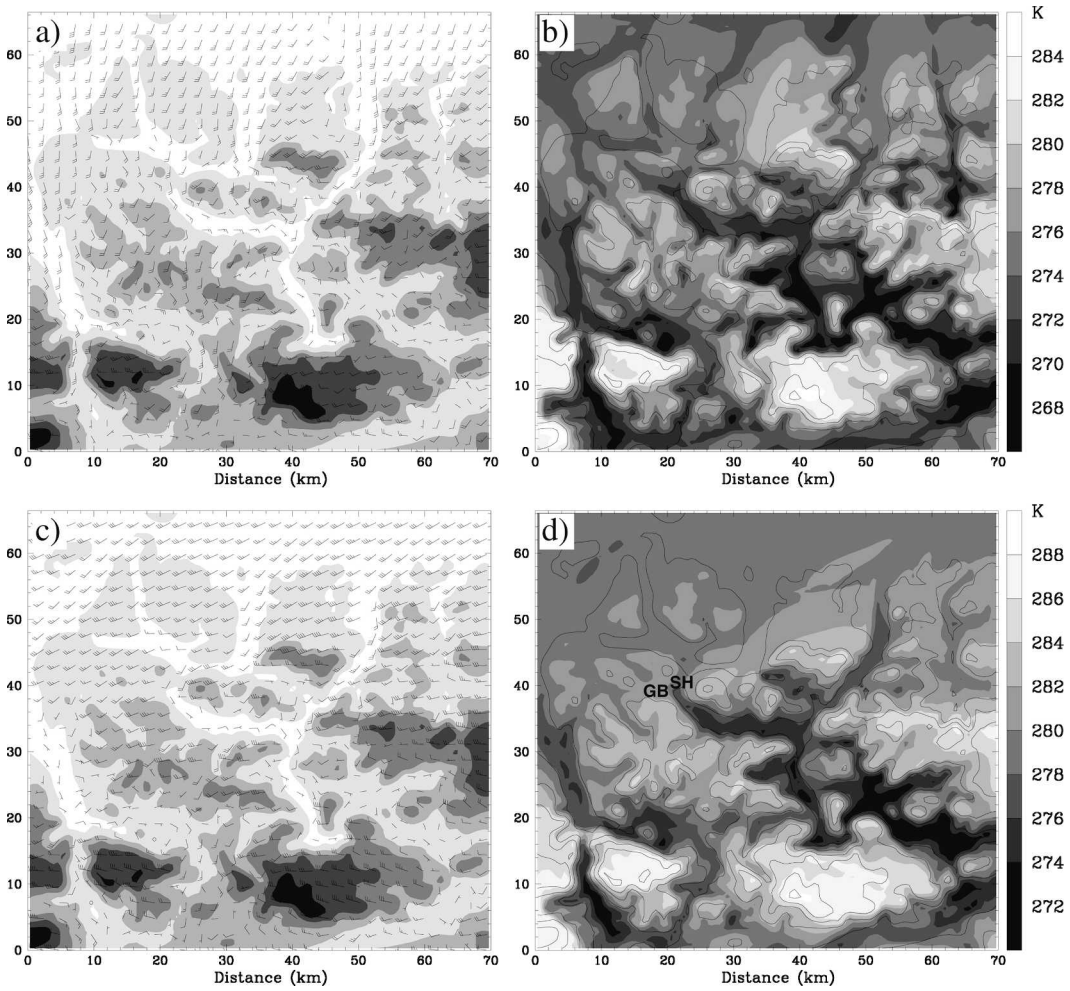

FIG. 5. (left) Wind field at 85 m AGL and (right) surface potential temperature at (a), (b) 2200 UTC 27 Dec and (c), (d) 0600 UTC 28 Dec. For the wind field, a full barb corresponds to 5 m s^{-1}, and topography is shaded as in Fig. 1b. In the right panels, topography is contoured at an interval of 400 m, starting at 600 m, and potential temperature is given shaded with steps every 2 K. Note that the shading key differs between (b) and (d) (see label bars). In (d), the locations of Gilgner Berg (GB) and Scharflingerhöhe (SH) are repeated from Fig. 1b.

except for Ramsau where the model produced 10 mm of precipitation. A very large discrepancy was found for the Feuerkogel, where the model produced 36 mm, while only 6 mm were reported by the station. However, this discrepancy is likely to be dominated by undercatch errors, since a sustained wind speed of 20–23 m s^{-1} (gusts up to 40 m s^{-1}) does not allow for a meaningful measurement of snowy precipitation with conventional rain gauges. Wind-related undercatch probably also played a role at Ramsau.

c. *Model results*

The primary question arising from the observations presented above is how the cold pool could be maintained for such a long time in the inner-Alpine valleys while it was quickly destroyed in the Alpine foreland. In addition, it remains to be discussed why the radiative cooling in the evening of 27 December was mainly restricted to the Alpine valleys, and why the surface potential temperature tends to be higher along the northern edge of the Alps (Gmunden) than farther north in the foreland (Wolfsegg and Linz). These issues will now be investigated on the basis of the model results.

We start our analysis at 2200 UTC on 27 December, roughly corresponding to the time when the warming begins at the valley stations and in the Alpine foreland (see Fig. 3). For this time, Figs. 5a and 5b display the wind field at about 85 m AGL and the potential temperature field at surface level for the innermost model domain. The wind field shows that the approach of the

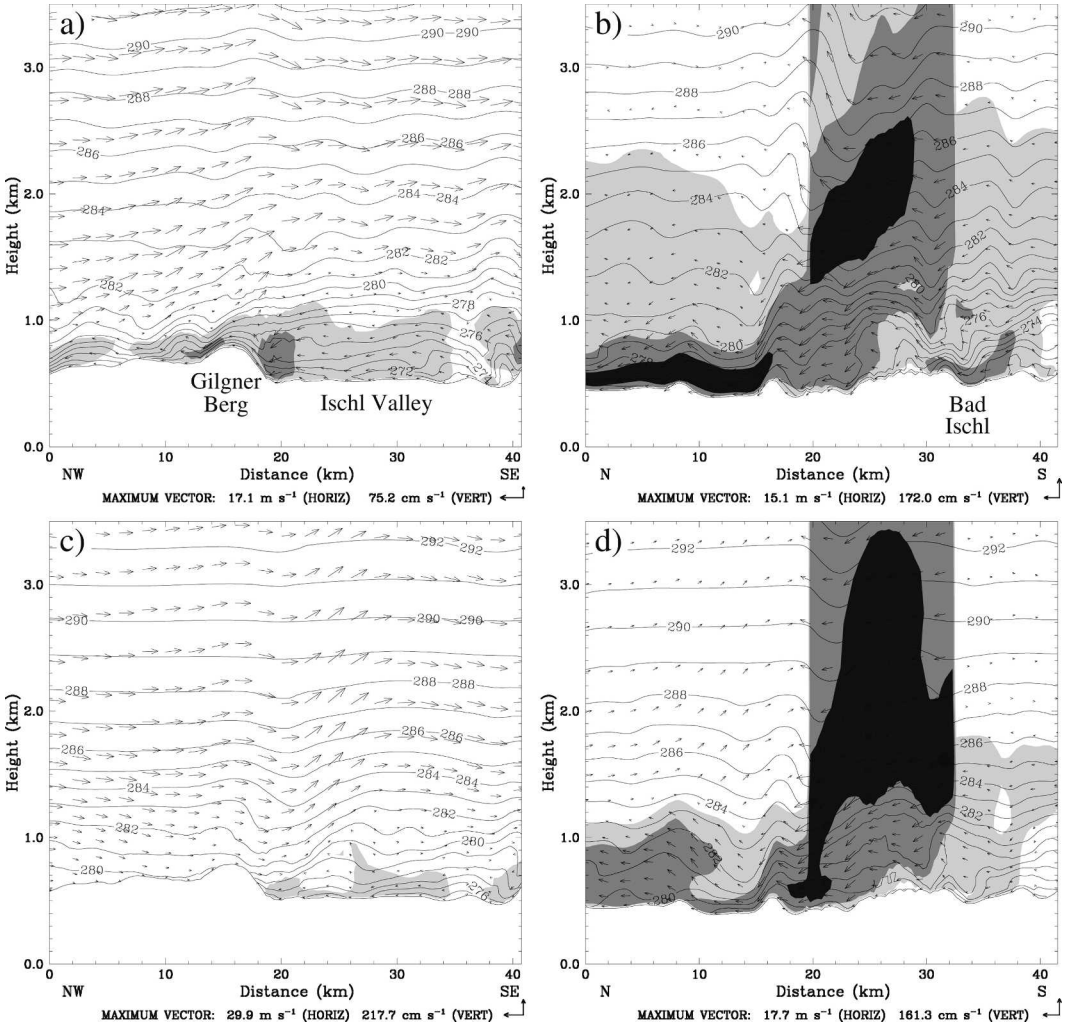

FIG. 6. Vertical cross sections of potential temperature (contour interval 1 K) and wind component parallel to the cross section (vectors) along lines (left) a1–a2 and (right) b1–b2 (see Fig. 1b for location). Note that the baselines of the cross sections have kinks in order to follow the valleys; they are located at 26 km for line a1–a2 and at 20 and 32 km for line b1–b2. Thus, the shading indicating the projected wind component may appear discontinuous there. Results are valid at (a), (b) 2200 UTC 27 Dec and (c), (d) 0600 UTC 28 Dec. Winds directed toward the Alpine foreland are shaded if exceeding 4 m s^{-1} with steps every 4 m s^{-1}.

warm front is associated with pronounced southerly flow in the Alpine foreland. This agrees well with the larger-scale field depicted in Fig. 2b, where the wind direction also shifts to south in the frontal region. Moreover, the southerly direction of the low-level flow helps understanding of why the warming commences earliest along the northern edge of the Alps. Being directed away from the Alps, the southerly flow is associated with pronounced subsidence and therefore advects potentially warm air from higher levels to the Alpine foothills while the preexisting cold air is pushed out into the foreland. In the Alpine valleys, the model results indicate a general cold-air outflow toward the Alpine foreland. However, the speed of this drainage flow is quite low at most places, which readily explains why the radiative cooling in the preceding hours was much more effective in the valleys than in the foreland. Comparison of Figs. 5a and 5b also shows that the coldest temperatures are correlated with the lowest wind speeds.

Further information on the vertical structure of the cold-air outflow is provided in the upper panels of Fig. 6. The cross section along line a1–a2 in Fig. 6a (see Fig. 1b for location) shows that the easterly outflow along the Ischl Valley has a depth of about 500 m and an average speed between 5 and 6 m s^{-1}. Note that this cold-air outflow is directed upvalley, thereby differing from a classical radiation-induced drainage flow, and

has an angle of slightly more than 90° to the ambient geostrophic wind direction. Near 20 km on the abscissa of Fig. 6a, the outflow splits into two branches, which renders the flow rate appearing in Fig. 6a discontinuous. One part exits into the Alpine foreland via a pass named Gilgner Berg and thus follows the cross section, while the other part takes its way over a somewhat lower pass named Scharflingerhöhe (Fig. 5a; see Figs. 1b or 5d for location). Above the cold-air outflow layer, the static stability is quite low in the Alpine foreland because of the subsidence related to the southerly flow.

Along the Traun Valley (cross section b1–b2; Fig. 6b), a more complex flow pattern appears because this valley has pronounced variations of its width. Moreover, the valley has two major kinks that have to be followed by the base line of the cross section (see Fig. 1b), rendering the wind speed projected onto the valley axis discontinuous. At low levels, a downvalley flow with up to 10 m s^{-1} appears south of Bad Ischl, but the near-surface flow speed gets markedly reduced north of this place. This is mainly due to the junction with the Ischl Valley, into which part of the drainage flow branches off. In addition, the Traun Valley has a pronounced lateral constriction north of Bad Ischl, which also has the consequence that the coldest low-level air remains partly blocked in the inner-Alpine part of the valley. North of this constriction, around km 25 on the abscissa of Fig. 6b, a gradual subsiding motion starts to develop in the Traun Valley, turning into a shooting hydraulic flow after the final constriction at 16 km. Note again that the static stability above the drainage flow layer is quite low in the northern part of the cross section.

The corresponding fields at 0600 UTC on 28 December are displayed in the lower panels of Figs. 5 and 6. The most obvious change in the wind field (Fig. 5c) is that the wind in the Alpine foreland has intensified and turned from south to southwest. Moreover, the cold-air outflow has weakened in most Alpine valleys, and the wind direction at the high mountain peaks now has a northerly component. Figure 5d shows that most Alpine valleys are still filled with cold air, while the temperature in the Alpine foreland is generally high without significant remnants of the previous cold air (note that the shading key in Fig. 5d had to be adapted to the higher temperature level). Particularly warm air reaches the Alpine foreland around Gmunden because of subsidence from the hill range to its west. As a consequence, the potential temperature at Gmunden is still higher than at Wolfsegg (see Fig. 3). The vertical cross section shown in Fig. 6c confirms that the cold-air outflow along the Ischl Valley is substantially weaker than at 2200 UTC on the previous day. Moreover, the outflow is now restricted to the Scharflingerhöhe pass (Fig. 5c) while southwesterly winds prevail at the Gilgner Berg. Along the Traun Valley (Fig. 6d), there is still appreciable outflow, but the low-level wind speeds in the southern part of the section (south of Bad Ischl) have weakened.

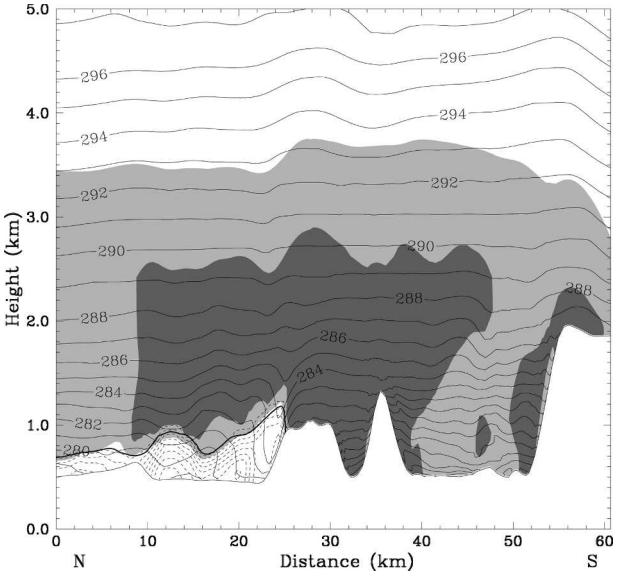

FIG. 7. Vertical cross section of potential temperature (solid lines; contour interval 1 K), snow mixing ratio (shading; increment 0.1 g kg^{-1}; white below 0.1 g kg^{-1}), and rain mixing ratio (dashed lines; contour interval 0.02 g kg^{-1}) along line c1–c2 (see Fig. 1b). Results are shown for 0600 UTC 28 Dec. The bold line marks the 0°C isotherm.

An important consequence of the cold-air trapping in the inner-Alpine valleys is that the precipitation related to the warm front reaches the valleys as snow while rain is falling in the Alpine foreland. This is illustrated in Fig. 7, showing the simulated mixing ratios of rain and snow at 0600 UTC. The freezing level, indicated by a bold line in Fig. 7, ranges between 700 and 1100 m in the foreland, but the temperature is generally below freezing in the inner-Alpine part of the section. Note in particular that the freezing level increases toward the northern Alpine edge due to the subsidence effects already discussed above.

The simulated fields at 1200 UTC (Figs. 8 and 9) reveal that the structural changes in the temperature field become very gradual during the day of 28 December. There is a slow, general warming trend both in the Alpine foreland and in the inner-Alpine valleys (see also Fig. 3), but the spatial extent of the cold pools undergoes only minor changes. This is also valid for the remaining 6 h of the integration time (not shown). Since the near-surface wind speed in the Alpine foreland is still above 15 m s^{-1}, the question arises why the re-

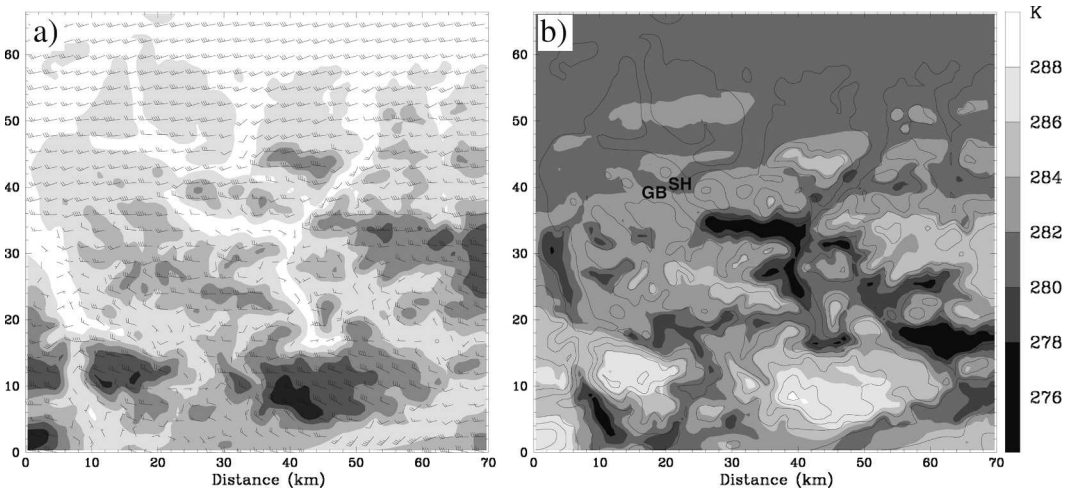

FIG. 8. Same as Fig. 5, but for 1200 UTC 28 Dec. In (b), the locations of Gilgner Berg (GB) and Scharflingerhöhe (SH) are repeated from Fig. 1b.

moval of the cold air in the Alpine valleys becomes so slow.

According to the model results, the crucial point seems to be that the cold-air loss toward the Alpine foreland has almost ceased. Compared to 0600 UTC, the cold pool in the Ischl Valley has somewhat retreated to the east (Fig. 8b), implying that there is no longer a cold-air outflow through the Scharflingerhöhe pass (Figs. 8a and 9a). Moreover, the downvalley flow appearing in the Traun Valley north of Bad Ischl is no longer associated with a noticeable outflow of cold air. As can be seen in Fig. 9b, significant downvalley flow is restricted to the valley segment north of Bad Ischl while winds are very weak farther south, and the low-level cold air lying south of Bad Ischl is not incorporated into the outflow. The downvalley flow in the Traun Valley rather seems to originate from levels above the cold pool, being the continuation of a westerly flow following the Ischl Valley and getting deflected into the Traun Valley at Bad Ischl (see also Figs. 11c,d). Although there is no direct observational evidence for this flow pattern, it is consistent with the maintenance of the near-surface temperature contrast (Fig. 3) and with the sustained southerly flow observed at Gmunden (not shown).

The quasi-stationarity of the cold pool after the cessation of the drainage flow also implies that turbulent

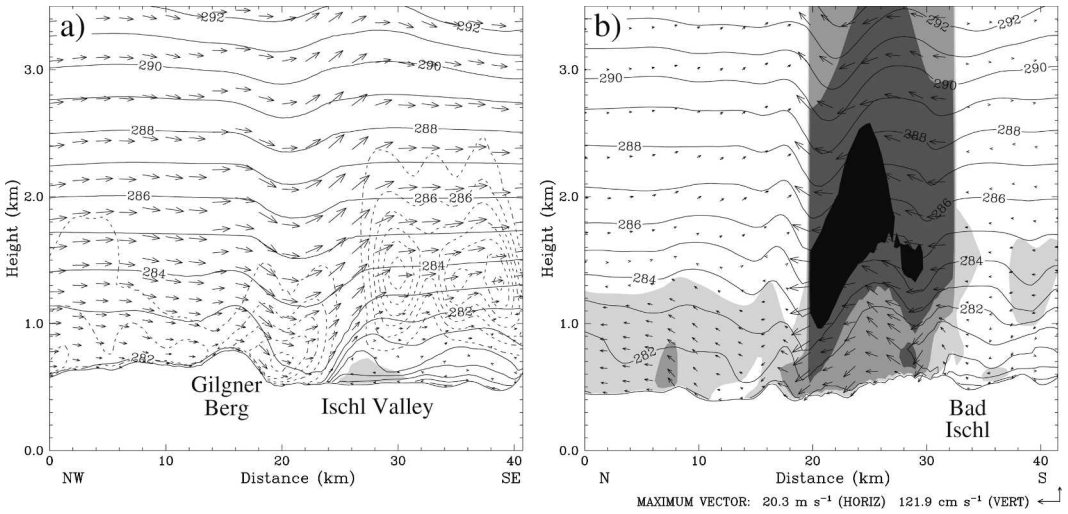

FIG. 9. Same as Fig. 6, but for 1200 UTC 28 Dec. The dashed lines in (a) indicate turbulent kinetic energy, with contour interval 1 $m^2 s^{-2}$ and first contour at 0.5 $m s^{-2}$. Note again that the cross sections do not follow straight lines (see Fig. 1b), which may render the wind component projected onto the cross section (vectors and shading) discontinuous.

mixing on top of the cold pool does not have a major impact. Even though the TKE field indicates the presence of substantial shear-induced turbulence above the cold pool (dashed lines in Fig. 9a), the turbulent mixing apparently does not penetrate far enough into the cold air to be really effective. For completeness, it is mentioned that radiative effects remained small throughout most of 28 December due to a closed cloud cover. In the evening, the clouds became somewhat thinner so that slight radiative cooling was possible in calm areas.

It remains to be discussed what controls the occurrence or absence of cold-air outflow into the Alpine foreland. From climatological data (e.g., monthly average temperatures), it can be inferred that the Salzkammergut region is by no means an exceptionally cold part of the Alps, indicating that cold-air trapping does not occur for a particularly wide spectrum of weather situations. Moreover, it is known that foehn occurs quite frequently in this region (e.g., Kuhn 1989), suggesting that the cold-air drainage into the Alpine foreland is more effective for southerly large-scale flow. These issues will be investigated in the subsequent section on the basis of idealized simulations with various large-scale wind directions.

4. Idealized experiments and dynamical analysis

a. Description of the results

An overview of the simulated surface potential temperature fields at $t = 24$ h is provided in Fig. 10. Evidently, the spatial distribution of the cold air remaining after that time exhibits a strong dependence on the ambient wind direction. For 310° and 290°, the cold air is mainly restricted to the Ischl Valley and the Traun Valley south of Bad Ischl (Figs. 10a,b). The almost uniform potential temperature in the rest of the model domain is related to the neglect of moisture and radiation, which in reality help in maintaining a positive vertical gradient of potential temperature. For westerly (270°) flow, the spatial extent of the cold pool increases, now including parts of the lower Traun Valley and the elevated region between Bad Aussee and Bad Mitterndorf (Fig. 10c). However, the intensity of the cold pool in the Ischl Valley weakens. This trend continues when turning the wind to 250° (Fig. 10d). With a further increase of the southerly wind component, the cold air shifts more and more into the Alpine foreland. For a wind direction of 230°, there are still some valley segments filled with cold air (Fig. 10e), but the cold air fully retreats into the foreland at a direction of 210° (Fig. 10f). In the latter case, downslope foehn flow dominates in the Alpine valleys.

To relate these idealized results to the case-study simulation discussed above, recall that the ambient wind direction in the Alpine region was slightly north of 270° during the day of 28 December (Figs. 2c,e). It is therefore quite encouraging that the quasi-steady state obtained from the case study (Fig. 8b) shows fairly similar structures as the idealized runs for 270° and 290°. Specifically, the cold pools in the Ischl Valley and in the Traun Valley are present in both idealized runs and in the case study, and the cold pool in the eastern Salzkammergut (Bad Aussee–Bad Mitterndorf) is reproduced at least in the 270° run. The strength of the cold pools found for the 270° run in the Traun Valley and in the eastern Salzkammergut is roughly similar to the case-study result, but the cold pool in the Ischl Valley tends to be weaker in the 270° run, combined with significant outflow into the Alpine foreland. In the latter valley, the cold-pool strength obtained from the 290° run more closely resembles the case-study result. The similarity between idealized and realistic model results confirms that the ambient wind direction is a crucial factor in determining the spatial structure of the cold-air pools, so that a further analysis of the idealized simulations can provide valuable insight into the underlying dynamics.

For the 290° run, Fig. 11a shows the wind and perturbation pressure fields at a constant height of 850 m. In the MM5 equations, the perturbation pressure represents the difference between the actual pressure and a reference pressure that depends on height only, implying that horizontal gradients of the perturbation pressure are true pressure gradients. The wind field in Fig. 11a shows a strong westerly wind with about 15 m s^{-1} in the Alpine foreland, which is between 3 and 4 m s^{-1} more than the large-scale wind speed specified at that height. This speedup is related to the flow deflection around the Alps, leading to the formation of a barrier jet along the Alps. The (perturbation) pressure tends to be higher in the Alpine valleys than in the foreland, with the lowest values occurring in the northeastern part of the domain. Outside the cold-pool areas, the spatial pressure differences are mainly related to orographic lifting of the air on the western side of the individual mountain ranges and to the subsequent downslope motion over the eastern slopes. Another contribution arises from the synoptic-scale pressure field, which imposes a general pressure decrease toward the north.

An inspection of the passes bordering the Ischl Valley to the west reveals that there is no cold-air outflow across the Gilgner Berg and at best a slight indication of cold-air outflow through the Scharflingerhöhe pass (Figs. 10b and 11a). For the Gilgner Berg, the lack of a cold-air outflow is obviously related to the fact that the

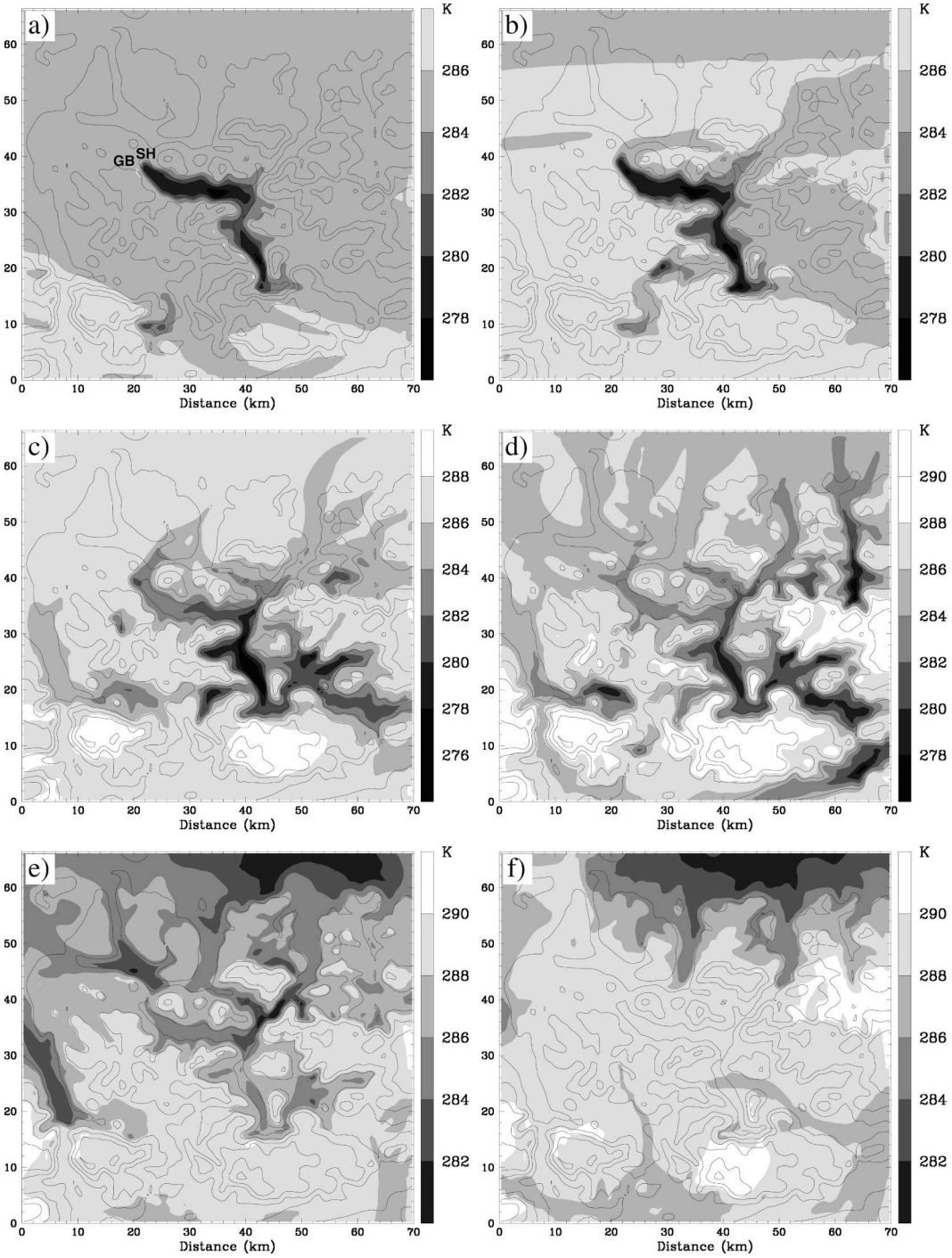

FIG. 10. Surface potential temperature at $t = 24$ h for semi-idealized simulations with a wind direction of (a) 310°, (b) 290°, (c) 270°, (d) 250°, (e) 230°, and (f) 210°. Topography is contoured every 400 m, starting at 600 m. Note that the shading key changes between (d) and (e). In (a), the locations of Gilgner Berg (GB) and Scharflingerhöhe (SH) are repeated from Fig. 1b.

cold pool does not reach up to this pass (Fig. 11b). However, the Scharflingerhöhe pass (~620 m in the model topography) is clearly below the top of the cold pool, and nevertheless does not carry a significant outflow. For this pass, the model results suggest that the reason lies in the absence of a noticeable pressure gradient across the pass, which in turn is related to upslope motion north of the pass. Specifically, the low-level

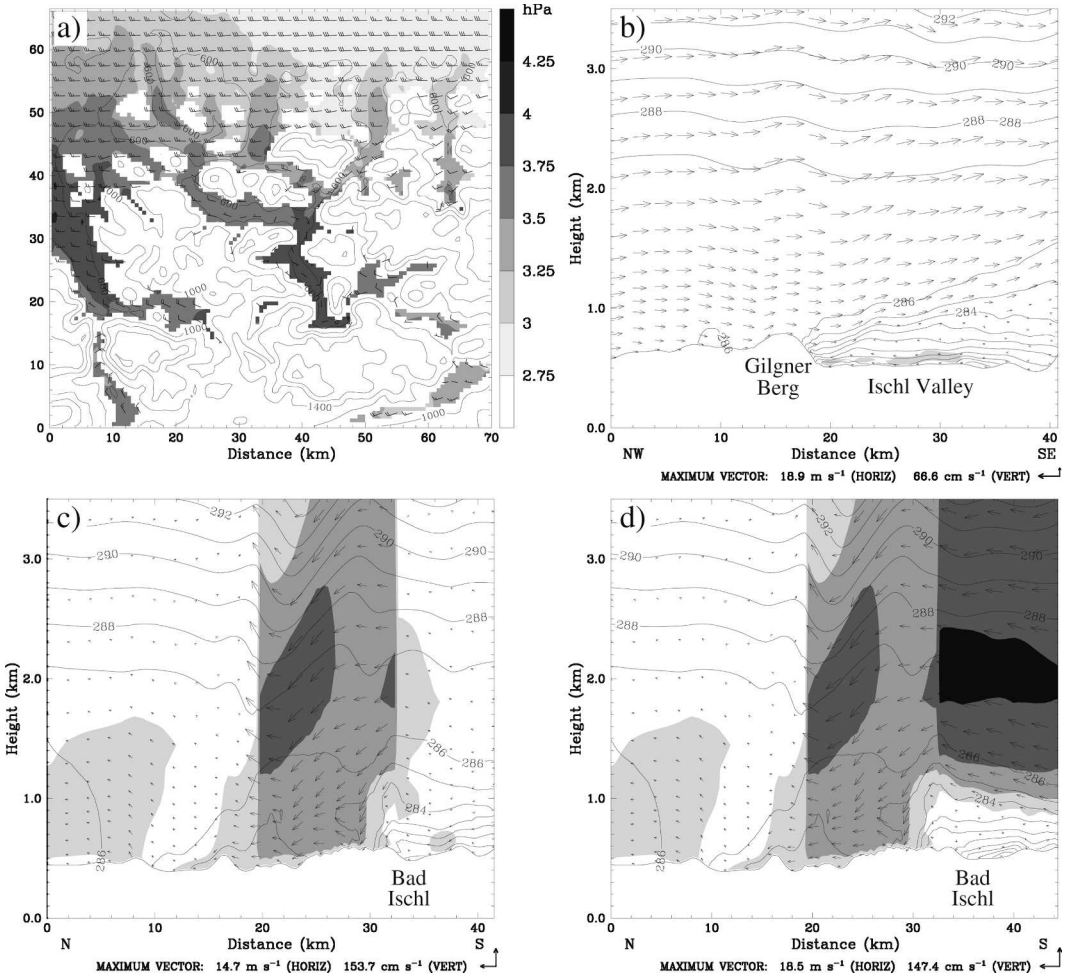

FIG. 11. Results for the 290° simulation at $t = 24$ h. (a) Wind field (full barb 5 m s^{-1}) and perturbation pressure (shading increment 0.25 hPa; see shading key) at a height of 850 m. Topography is contoured as in Fig. 10. Vertical cross sections of wind and potential temperature along lines (b) a1–a2, (c) b1–b2, and (d) b1–b3. Plotting conventions are as in Fig. 6.

flow arriving from the west is lifted over the mountain ridges east and northeast of the Scharflingerhöhe, as the valley in between is too narrow to transport all the flow. This induces a small local pressure maximum north of the Scharflingerhöhe (not evident in Fig. 11a because of the finite shading increment) that almost offsets the thermal pressure gradient across the pass.

Along the Traun Valley (Fig. 11c), the flow pattern is quite similar to the case-study result shown in Fig. 9b. There is a strong channeled flow along the valley segment north of Bad Ischl but almost no outflow farther south, and the cold air lying there is largely trapped. Note again that the Traun Valley has a pronounced lateral constriction north of Bad Ischl, which is essential for this cold-air trapping. To clarify the origin of the outflow appearing in the Traun Valley, Fig. 11d shows an additional cross section along line b1–b3 (see Fig. 1b), ending in the Ischl Valley rather than in the southern part of the Traun Valley. Evidently, the outflow is fed by the westerly airflow following the Ischl Valley above the cold pool. As such, it constitutes a return flow of warm air originating in the Alpine foreland rather than a true outflow of air originating in the valleys.

The 850-m wind and perturbation pressure field for the 270° simulation is displayed in Fig. 12a. A comparison with the 290° case reveals that the wind speed in the Alpine foreland is somewhat weaker for a direction of 270°. This is related to the fact that a direction of 270° is almost parallel to the Alpine base line, implying that only a weak barrier-jet formation is possible. Moreover, the tendency for northwesterly flow along the more elevated eastern Salzkammergut (Bad Aussee–Bad Mitterndorf) is much weaker, which explains why this

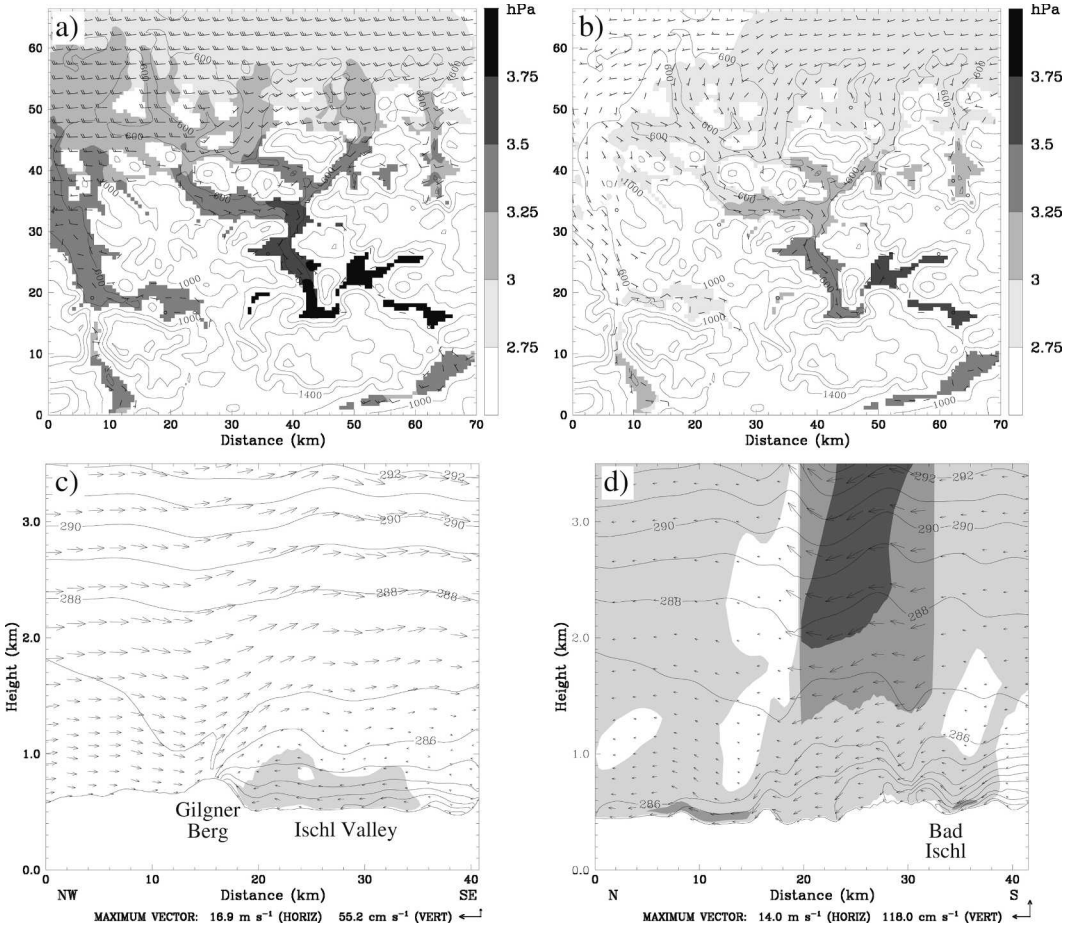

FIG. 12. (top) Same as Fig. 11a, but for simulations with a wind direction of (a) 270° and (b) 250°. (bottom) Vertical cross sections of wind and potential temperature along lines (c) a1–a2 and (d) b1–b2 for a wind direction of 270°, with plotting conventions as in Fig. 6. Results are valid at $t = 24$ h.

valley section now keeps a cold pool. On the other hand, a noticeable outflow through the Scharflingerhöhe pass appears in the 270° run, driven by a pressure difference across the pass of about 0.2 hPa (Fig. 12a). In this case, the upslope lifting north of the Scharflingerhöhe is too weak to compensate the pressure gradient induced by the low-level temperature difference. Consequently, the cold pool in the western Ischl Valley is less intense than in the 290° case (Figs. 10c and 12c). The flow along the Traun Valley now constitutes a true cold-air outflow, but the valley constriction north of Bad Ischl still manages to trap most of the cold air to its south (Fig. 12d).

A shift of the wind direction to 250° brings about a pronounced reduction of the wind speed in the Alpine foreland (Fig. 12b). The ambient flow is now directed away from the northern side of the Alps, leading to the formation of a wake with comparatively weak low-level winds. However, the winds in the foreland are still strong enough to advect away the initial cold air (Fig. 10d). In the Alpine Valleys, one finds a general drainage flow toward the foreland that follows the mesoscale pressure gradient without being disturbed by interactions with an ambient westerly flow.

As already mentioned, further increasing the southerly wind component leads to a substantial change of the temperature pattern (Figs. 10e,f). While the cold air in the Alpine valleys disappears, a persistent cold pool is now found in the Alpine foreland. The latter is related to the wake effect in the lee of the Alps, which is now strong enough to prevent a downstream advection of the initial cold air. Since the removal of the cold air in the Alpine valleys takes only about 15 h in the 210° run, we consider the model results at $t = 6$ h in order to examine the erosion process in more detail. The cross section a1–a2 along the Ischl Valley (Fig. 13a) indicates a deep southeasterly outflow of cold air, reaching up to a height of more than 1500 m. The outflow speed typi-

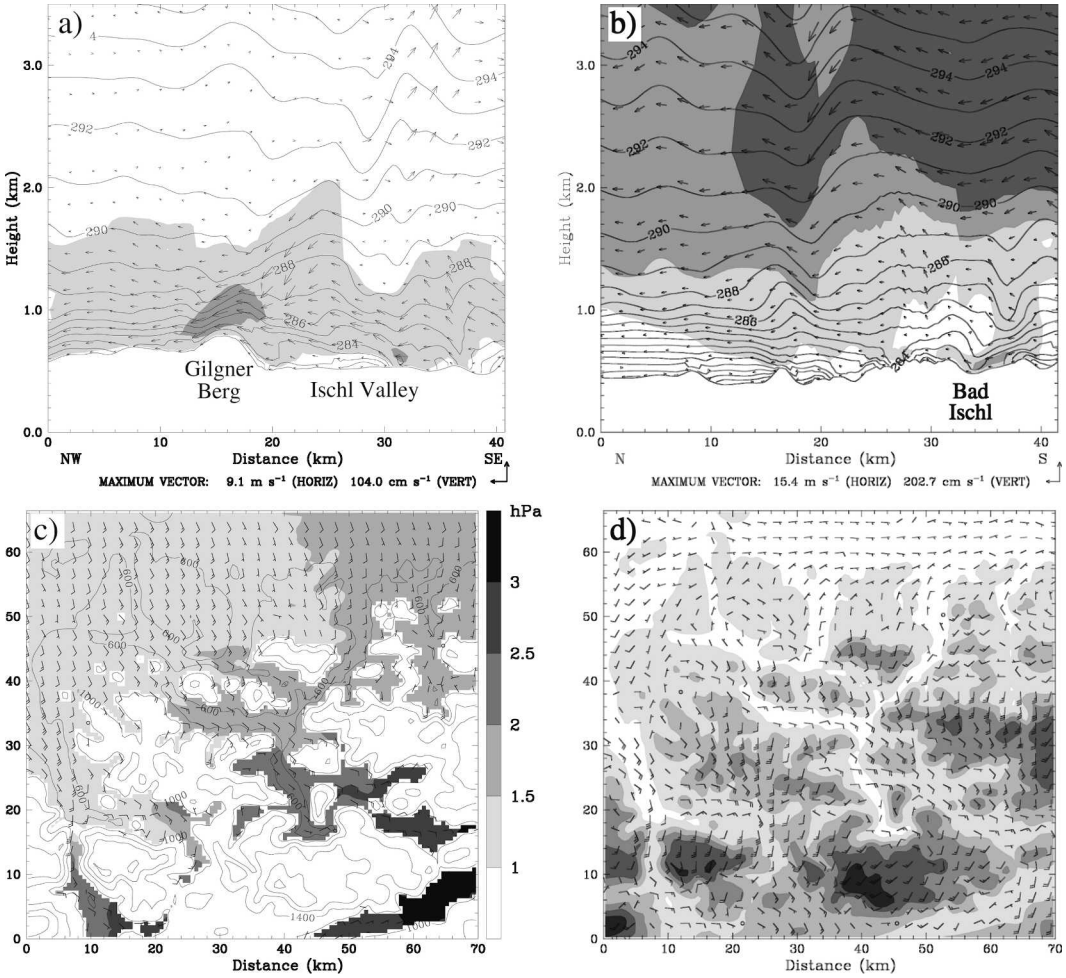

FIG. 13. Results for the 210° simulation. (top) Vertical cross sections of wind and potential temperature along lines (a) a1–a2 and (b) b1–b2 at $t = 6$ h with plotting conventions as in Fig. 6. (c) Wind field and perturbation pressure at a height of 1000 m, $t = 6$ h, and plotting conventions as in Fig. 11a. (d) Wind field at 85 m AGL, $t = 24$ h, and plotting conventions as in Fig. 5a.

cally ranges between 5 and 8 m s^{-1}. The wind field at $z = 1000$ m (Fig. 13c) confirms the presence of a general southeasterly outflow, which is deeper and more intense than for westerly large-scale flow. It is driven by a northwestward-directed pressure gradient force (Fig. 13c), which is related to a superposition of cold-pool effects and the synoptic-scale pressure field. Note also that the shading increment in Fig. 13c is twice as large as in the preceding figures, implying that the outward pressure gradient force is substantially stronger than in the previous cases. Along the Traun Valley, a southwesterly outflow is found, but its low-level speed is smaller than for the southeasterly flow along the Ischl Valley (Figs. 13b,c). It is also important to note that the low-level static stability along the Traun Valley is much higher in the Alpine foreland than in the inner-Alpine part (Fig. 13b), implying that the main cold-air loss takes place along the Ischl Valley.

The final ($t = 24$ h) flow field at 85 m AGL for the 210° case is shown in Fig. 13d. It reveals that southeasterly flow still prevails in the inner-Alpine valleys. Moreover, there is a tendency for the formation of wind maxima over the northern slopes of the individual mountain ranges, which is related to orographic gravity waves. Without presenting detailed evidence, it is mentioned that the gravity-wave-induced downslope acceleration of the flow also contributes to the rapid removal of the cold air because the ensuing high low-level wind speeds favor turbulent erosion. In the Alpine foreland, an easterly ageostrophic flow is found within the cold pool, which is a very typical feature accompanying foehn in the Alps.

b. Interpretation

Taking these results together, it can be summarized that the dependence of the cold-pool behavior on the large-scale wind direction results from a complex interaction between the mesoscale pressure field and the valley geometry. For the Ischl Valley and the inner-Alpine part of the Traun Valley, the most effective drainage paths are located on the western edge (Gilgner Berg and Scharflingerhöhe). These passes have a wide cross section and thus can transport substantial amounts of air, implying that ambient conditions favorable for easterly ageostrophic flow will lead to a rapid cold-air outflow. The lower Traun Valley has, although not leading over a pass, a lower capacity because of pronounced lateral constrictions of the valley width. Therefore, ambient conditions allowing for cold-air outflow through the Traun Valley only lead to a much higher persistence of the inner-Alpine cold pool. Such conditions are given for westerly and northwesterly large-scale flow (and probably also for northerly flow, which was not investigated here because warm-air advection from the north is quite unlikely). A slightly different situation arises for the valley between Bad Aussee and Bad Mitterndorf. This valley has outflow paths in the northwest and in the southeast, implying that northwesterly ambient flow can be channeled along this valley and induce a downstream advection of the low-level cold air, possibly combined with some turbulent erosion. Consequently, this valley section exhibits the highest persistence of cold-air pools for westerly flow. On the other hand, both parts of the valley system have in common that the climatologically frequent situation of warm-air advection from the southwest induces a rapid outflow of the cold air, which explains why the average winter temperatures are not particularly low.

A comparison of the idealized results with the temporal evolution of the case-study simulation confirms the strong relationship between the drainage-flow behavior and the low-level wind direction. During the initial part of the event (evening of 27 December), a substantial cold-air outflow was found to occur via the Gilgner Berg and the Scharflingerhöhe pass (Figs. 5a and 6a), consistent with the presence of southerly to southwesterly low-level flow at that time. Later on, as the ambient flow turned to about 280°, the outflow rate decreased to a very small level. This implies that the maintenance of a cold pool in the Alpine valleys was strongly related to the fact that the phase of southwesterly ambient flow lasted only for a few hours. Moreover, as opposed to the idealized simulations without directional shear, the southwesterly flow in the real case was quite shallow (see Fig. 2a). Therefore, the depth of the cold-air outflow appearing in the real case (Fig. 6a) was substantially smaller than in the idealized 210° case (Fig. 13a), which constitutes another important factor for the maintenance of the cold pool.

5. Conclusions

In this study, high-resolution numerical simulations have been presented in order to investigate dynamical aspects of wintertime cold-air pools in an Alpine valley system. The work comprises both a realistic case study and semi-idealized simulations combining real topography with idealized large-scale flow conditions. In the real case, the formation of the cold pool was related to the passage of a warm front, during which the preexisting cold air was removed in the Alpine foreland but not in the inner-Alpine part of the valley system. This evolution was mimicked in the idealized simulations by exposing an initial cold pool to an ambient flow with a range of different directions, aiming at examining the relationship between the cold-pool evolution and the ambient wind direction. The simulations have been conducted with the fifth-generation Pennsylvania State University–National Center for Atmospheric Research Mesoscale Model (MM5), including a number of modifications to improve the model accuracy over mountainous terrain.

The first conclusion that can be drawn from this work is that the MM5—at least with the modifications implemented by the author—is capable of simulating cold-air pools in deep Alpine valleys with remarkable accuracy. Though there appears a slight warm bias at some inner-Alpine stations, the model captures on average about 80% of the temperature difference observed between the Alpine foreland and the valleys. Therefore, the model results are certainly adequate for studying the dynamical mechanisms underlying such cold-pool events.

Regarding the dynamical mechanisms affecting cold-air pools in a deep valley system, the model results suggest that drainage flows following the local pressure gradient are the most efficient mechanism of cold-air removal. This essentially confirms the findings made by Zängl (2003a) for a highly idealized valley topography, indicating that the leading importance of the drainage mechanism is robust with respect to topographic details. In addition, the present study revealed that the preferred direction of cold-air outflow is down the pressure gradient related to the ambient (geostrophically balanced) flow. Cold-air drainage along the direction of the ambient flow, which was the only pathway considered in the earlier study, is also possible but requires a

mechanism that generates a suitable along-valley pressure gradient. The most likely candidate for this is gravity-wave-induced subsidence of potentially warm air along the northern edge of the Alps, which takes some finite time to develop and therefore might become effective only if a more favorable outflow path is missing. Moreover, the results of this work reveal that the geometry of the possible flow pathways into the foreland (valleys or low passes) plays an important role for their drainage efficiency. In particular, the presence of pronounced lateral constrictions greatly reduces the cold-air outflow through a valley or pass. Taking both together, it follows that optimal conditions for cold-air drainage are given when the connecting valley or pass has a large width and points down the pressure gradient related to the ambient (geostrophically balanced) flow. For the valley system considered in this study, these conditions are fulfilled for southwesterly large-scale flow, as the widest connection to the Alpine foreland is directed toward the northwest. The other main connection to the Alpine foreland, leading down the Traun Valley to the northeast, is much less effective because of lateral valley constrictions. Therefore, westerly and northwesterly large-scale flow conditions favor the maintenance of cold-air pools.

Compared to the drainage mechanism, cold-pool erosion by turbulent mixing seems to play a comparatively minor role for deep mountain valleys as considered in this study. This is in basic accordance with Zhong et al. (2003), although turbulent mixing is probably not as ineffective as suggested by their simplified analytical model. The results presented in Zängl (2003a) suggest that turbulent mixing can be important for shallow cold pools, particularly in basins having no or no significant outflow. Moreover, turbulent erosion may become relevant when the formation of orographic gravity waves accelerates the ambient airflow down into a valley and maintains very strong vertical shear on top of the cold pool.

What remains to be done in future studies is proving the generality of these results, for example, by conducting similar investigations for other valley systems. If the strong link between the ambient wind direction and the persistence of local cold-air pools turns out to be a general feature in Alpine valleys, this would have interesting implications for local weather forecasting in mountainous areas. To refine the output fields of the operational forecasts, which are intrinsically unable to represent small-scale cold-air pools due to a lack of spatial resolution, one could then precompute high-resolution lookup charts for the relevant range of wind directions and use those charts as an additional guideline for local forecasting.

Acknowledgments. The author wants to thank the anonymous reviewers for their constructive comments that led to a significant improvement of this paper.

REFERENCES

Anquetin, S., C. Guilbaud, and J.-P. Chollet, 1998: The formation and destruction of inversion layers within a deep valley. *J. Appl. Meteor.,* **37,** 1547–1560.

Bader, D. C., and T. B. McKee, 1985: Effects of shear, stability and valley characteristics on the destruction of temperature inversions. *J. Climate Appl. Meteor.,* **24,** 822–832.

Clements, C. B., C. D. Whiteman, and J. D. Horel, 2003: Cold-air-pool structure and evolution in a mountain basin: Peter Sinks, Utah. *J. Appl. Meteor.,* **42,** 752–768.

Colette, A., F. K. Chow, and R. L. Street, 2003: A numerical study of inversion-layer breakup and the effects of topographic shading in idealized valleys. *J. Appl. Meteor.,* **42,** 1255–1272.

Garnier, B. J., and A. Ohmura, 1968: A method of calculating the direct shortwave radiation income of slopes. *J. Appl. Meteor.,* **7,** 796–800.

Grell, G. A., 1993: Prognostic evaluation of assumptions used by cumulus parameterizations. *Mon. Wea. Rev.,* **121,** 764–787.

——, J. Dudhia, and D. R. Stauffer, 1995: A description of the fifth-generation Penn State/NCAR Mesoscale Model (MM5). NCAR Tech. Note NCAR/TN-398+STR, 122 pp.

Klemp, J. B., and D. R. Durran, 1983: An upper boundary condition permitting internal gravity wave radiation in numerical mesoscale models. *Mon. Wea. Rev.,* **111,** 430–444.

Kuhn, M., Ed., 1989: *Föhnstudien (Foehn Studies).* Wissenschaftliche Buchgesellschaft, 504 pp.

Lee, T. J., R. A. Pielke, R. C. Kessler, and J. Weaver, 1989: Influence of cold pools downstream of mountain barriers on downslope winds and flushing. *Mon. Wea. Rev.,* **117,** 2041–2058.

Mlawer, E. J., S. J. Taubman, P. D. Brown, M. J. Iacono, and S. A. Clough, 1997: Radiative transfer for inhomogeneous atmosphere: RRTM, a validated correlated-k model for the longwave. *J. Geophys. Res.,* **102,** 16 663–16 682.

Petkovšek, Z., 1992: Turbulent dissipation of cold air lake in a basin. *Meteor. Atmos. Phys.,* **47,** 237–245.

——, and T. Vrhovec, 1994: Note on influences of inclined fog lakes on the air pollution in them and on the irradiance above them. *Meteor. Z.,* **3,** 227–232.

Rakovec, J., J. Merše, S. Jernej, and B. Paradiž, 2002: Turbulent dissipation of the cold-air pool in a basin: Comparison of observed and simulated development. *Meteor. Atmos. Phys.,* **79,** 195–213.

Reisner, J., R. M. Rasmussen, and R. T. Bruintjes, 1998: Explicit forecasting of supercooled liquid water in winter storms using the MM5 mesoscale model. *Quart. J. Roy. Meteor. Soc.,* **124,** 1071–1107.

Schär, C., D. Leuenberger, O. Fuhrer, D. Lüthi, and C. Girard, 2002: A new terrain-following vertical coordinate for atmospheric prediction models. *Mon. Wea. Rev.,* **130,** 2459–2480.

Shafran, P. C., N. L. Seaman, and G. A. Gayno, 2000: Evaluation of numerical predictions of boundary layer structure during the Lake Michigan Ozone Study (LMOS). *J. Appl. Meteor.,* **39,** 412–426.

Vrhovec, T., 1991: A cold air lake formation in a basin—A simulation with a mesoscale numerical model. *Meteor. Atmos. Phys.,* **8,** 91–99.

Whiteman, C. D., 1982: Breakup of temperature inversions in deep mountain valleys. Part I: Observations. *J. Appl. Meteor.,* **21,** 270–289.

——, and T. B. McKee, 1982: Breakup of temperature inversions in deep mountain valleys. Part II: Thermodynamic model. *J. Appl. Meteor.,* **21,** 290–302.

——, T. Haiden, B. Pospichal, S. Eisenbach, and R. Steinacker, 2004: Minimum temperatures, diurnal temperature ranges, and temperature inversions in limestone sinkholes of different size and shape. *J. Appl. Meteor.,* **43,** 1224–1236.

Zängl, G., 2002a: Stratified flow over a mountain with a gap: Linear theory and numerical simulations. *Quart. J. Roy. Meteor. Soc.,* **128,** 927–949.

——, 2002b: An improved method for computing horizontal diffusion in a sigma-coordinate model and its application to simulations over mountainous topography. *Mon. Wea. Rev.,* **130,** 1423–1432.

——, 2003a: The impact of upstream blocking, drainage flow and the geostrophic pressure gradient on the persistence of cold air pools. *Quart. J. Roy. Meteor. Soc.,* **129,** 117–137.

——, 2003b: A generalized sigma coordinate system for the MM5. *Mon. Wea. Rev.,* **131,** 2875–2884.

Zhong, S., C. D. Whiteman, X. Bian, W. J. Shaw, and J. M. Hubbe, 2001: Meteorological processes affecting the evolution of a wintertime cold air pool in the Columbia basin. *Mon. Wea. Rev.,* **129,** 2600–2613.

——, X. Bian, and C. D. Whiteman, 2003: Time-scale for cold-air pool breakup by turbulent erosion. *Meteor. Z.,* **12,** 229–233.